Research article

Sarath Raman Nair*, Lachlan J. Rogers, Xavier Vidal, Reece P. Roberts, Hiroshi Abe, Takeshi Ohshima, Takashi Yatsui, Andrew D. Greentree, Jan Jeske and Thomas Volz

Amplification by stimulated emission of nitrogen-vacancy centres in a diamond-loaded fibre cavity

https://doi.org/10.1515/nanoph-2020-0305
Received May 26, 2020; accepted August 23, 2020; published online September 28, 2020

Abstract: Laser threshold magnetometry using the negatively charged nitrogen-vacancy (NV^-) centre in diamond as a gain medium has been proposed as a technique to dramatically enhance the sensitivity of room-temperature magnetometry. We experimentally explore a diamond-loaded open tunable fibre-cavity system as a potential contender for the realisation of lasing with NV^- centres. We observe amplification of the transmission of a cavity-resonant seed laser at 721 nm when the cavity is pumped at 532 nm and attribute this to stimulated emission. Changes in the intensity of spontaneously emitted photons accompany the amplification, and a qualitative model including stimulated emission and ionisation dynamics of the NV^- centre captures the dynamics in the experiment very well. These results highlight important considerations in the realisation of an NV^- laser in diamond.

Keywords: diamond colour centres; fibre cavity; laser threshold magnetometry; nitrogen-vacancy centres; NV charge state switching; NV-stimulated emission.

Current address: **Lachlan J. Rogers**, School of Mathematical and Physical Sciences, University of Newcastle, Newcastle, NSW 2308, Australia
Current address: **Takashi Yatsui**, Toyohashi University of Technology, Toyohashi, Aichi 441-8580, Japan

***Corresponding author: Sarath Raman Nair**, ARC Centre of Excellence for Engineered Quantum Systems (EQUS) and Department of Physics and Astronomy, Macquarie University, NSW 2109, Australia, E-mail: sarath.raman-nair@mq.edu.au. https://orcid.org/0000-0002-9081-5750
Lachlan J. Rogers, Reece P. Roberts and Thomas Volz, ARC Centre of Excellence for Engineered Quantum Systems (EQUS) and Department of Physics and Astronomy, Macquarie University, NSW 2109, Australia. https://orcid.org/0000-0003-3545-2595 (L.J. Rogers). https://orcid.org/0000-0001-9850-4992 (T. Volz)
Xavier Vidal, ARC Centre of Excellence for Engineered Quantum Systems (EQUS) and Department of Physics and Astronomy, Macquarie University, NSW 2109, Australia; Fraunhofer Institut für Angewandte Festkörperphysik (IAF), Tullastrasse 72, 79108 Freiburg, Germany. https://orcid.org/0000-0001-8026-2016
Hiroshi Abe and Takeshi Ohshima, National Institutes for Quantum and Radiological Science and Technology, Takasaki, Gunma, 370-1292, Japan. https://orcid.org/0000-0002-7850-3164 (T. Ohshima)
Takashi Yatsui, School of Engineering, University of Tokyo, Tokyo 113-8656, Japan
Andrew D. Greentree, ARC Centre of Excellence for Nanoscale BioPhotonics, School of Science, RMIT University, Melbourne, VIC 3001, Australia. https://orcid.org/0000-0002-3505-9163
Jan Jeske, Fraunhofer Institut für Angewandte Festkörperphysik (IAF), Tullastrasse 72, 79108 Freiburg, Germany; Chemical and Quantum Physics, School of Sciences, RMIT University, Melbourne 3001, Australia. https://orcid.org/0000-0003-3532-506X

1 Introduction

Quantum magnetic sensing is driving rapid development in applications ranging from life science to navigation technologies [1, 2] and is contributing to breakthroughs in fundamental physics [3–5]. Much of this effort over the last decade has made use of the negatively charged nitrogen-vacancy (NV^-) centre in diamond [1, 2, 6, 7], which is particularly attractive since it allows quantum measurements at ambient temperatures and provides nanoscale resolution [5, 8, 9]. The NV^- centre has spin-optical properties uniquely well suited for sensing applications [2] and offers magnetometry based on reliable control and optical read-out of magnetically sensitive ground state spin levels. Since the first theoretical proposals for NV^- spin magnetometry [10, 11] and the breakthrough demonstrations in experiments [12, 13], many different types of NV^- sensing modalities have been suggested and tested [1, 7].

While a range of experiments have been performed and real-world technical applications are already emerging, there is an ongoing quest to improve sensitivity. The best NV^- sensitivity reported so far is 0.9 $pT/\sqrt{Hz}$ [14], which is several orders of magnitude worse than initial expectations [1, 2, 10]. These extra orders of magnitude are required in order to reach the goal of sensitivities comparable to state-of-the-art superconducting quantum interference device (SQUID) technology [1, 2], which would open numerous

applications to room-temperature implementation. One of the key limiting factors is the shot noise that arises from the difficulty in efficiently detecting single photons [7]. This is particularly true for single-spin sensing applications, but it still plays a role when using an ensemble of NV^- spins to enhance the sensitivity. Ensemble magnetometry reduces spatial resolution [1, 7, 10], but many technical applications such as magnetic resonance imaging can sacrifice spatial resolution to gain sensitivity.

One proposal to bypass the photon shot-noise problem is a technique called laser threshold magnetometry, and it has the potential to improve sensitivity towards the $\mathrm{fT}/\sqrt{\mathrm{Hz}}$ regime [15, 16]. The main idea is to construct a laser using stimulated emission of NV^- centres in the phonon sideband and detect magnetic fields by the change in laser output power close to the threshold. An NV^- laser bypasses the shot noise problem since the detection of spontaneous photons is replaced by the detection of a weak coherent laser beam. The idea of using colour centres in diamond (and in particular, NV^- centres) as a laser gain medium has been around for a while [17–19]. To the best of our knowledge, the demonstration of an NV^- laser or even the stimulated emission of NV^- centres inside an optical cavity has not been achieved so far. However, recently, the first direct observation of stimulated emission from NV^- centres (without any optical cavity) has been reported as an important step [20].

Stimulated emission is vital for developing a laser, and yet some contention surrounds this phenomenon in NV^- centres. The main concern is the near-infrared (NIR)–induced photoionisation, which has recently attracted considerable interest [21–23]. Super-resolution microscopy using the stimulated emission depletion (STED) technique has been repeatedly demonstrated with NV^- centres [24–27], even for 1064-nm irradiation where the STED cross section should be negligible [28]. Importantly, the STED technique will achieve super-resolution with any mechanism that depletes the fluorescence of the NV^- centre upon irradiation of laser light, and so it does not prove the presence of stimulated emission. For example, photoionisation could be responsible for the quenching of fluorescence as has recently been described for low-power subdiffraction-limited microscopy using NV^- centres [21]. The charge state switching dynamics between negative and neutral charge states of the NV centre due to the NIR wavelengths have also been taken into account in exploring the avenue of direct NV^- stimulated emission [22, 29, 30]. This ionisation induced by NIR wavelengths naturally poses concerns about the realisation of the stimulated emission from NV^- centres and its amplification inside a strong optical cavity for NIR wavelengths.

Here, we demonstrate amplification of laser light transmitted through an open tunable fibre cavity [31] loaded with a diamond sample containing a high concentration of NV^- centres. A 721-nm laser was used to seed the cavity mode instead of relying on the amplification of spontaneously emitted photons from the NV centres. Optically pumping NV^- centres with an off-resonant 532-nm excitation led to the amplification of this seed laser transmission. This was accompanied by a reduction in the spontaneously emitted photons at other wavelengths, strongly supporting the conclusion of amplification by stimulated emission. A recovery of spontaneous emission at higher pump powers is interpreted in the light of NIR-induced photoionisation. We qualitatively model the observed cavity output dynamics by including charge state switching to NV^0 and find good agreement with the data. Using a seed laser made it possible to observe the interplay of stimulated emission and charge state dynamics in the presence of a cavity with lower requirements on the effective cavity quality factor. These results address the concern that the strong NIR intracavity field might induce charge state switching of NV^- to NV^0 to a degree that precludes an NV^- laser. Our analysis highlights the important parameters and processes occurring in the diamond samples that are currently limiting the realisation of an NV^- laser threshold magnetometer as originally proposed in Jan et al. [15].

This article has the following structure. The diamond sample and experimental fibre-cavity apparatus are introduced in Section 2. Section 3 presents the cavity transmission measurements showing optical amplification. A qualitative model is developed in Section 4, considering stimulated emission and charge state switching of NV centres. In Section 5, we discuss the experimentally observed amplification behaviour in the light of the qualitative model. The concluding Section 6 discusses the challenges ahead for achieving NV^- lasing.

2 Experimental details

The sample used in these experiments was a commercial type 1b high pressure high temperature (HPHT) diamond from E6 with [100] orientation, which was electron beam irradiated at 2 MeV to a fluence of 10^{18} cm^{-2}. This was performed in vacuum and at a temperature of 740 °C in order to achieve *in situ* annealing, which improves NV creation [32] to a concentration of 1.7 ppm.

This corresponds to an effective density of NV centres of 3×10^{17} cm^{-3}, which is the number used in our models in the remainder of the paper. The sample was then laser cut

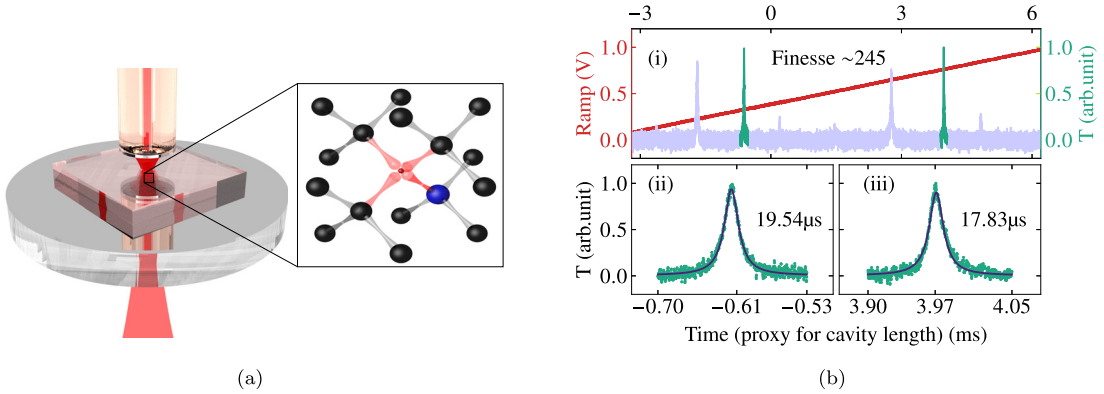

Figure 1: The diamond-loaded fibre cavity platform. (a) Schematic of the fibre cavity loaded with a diamond sample containing nitrogen-vacancy (NV) centres. The diamond sample is placed on top of the macroscopic mirror, and a concave fibre-end mirror is approached from the top forming a stable Fabry–Perot microcavity. The inset displays the structure of the NV^- centre within the diamond lattice. Black spheres are carbon atoms, blue indicates nitrogen, and red illustrates the dangling bonds that form electron orbitals around the vacancy position. (b) The cavity finesse was measured by applying a triangular voltage ramp (red) to the piezo in order to tune the cavity length by moving the fibre. The cavity transmission T was measured (shown here normalised to the maximum value), and multiple peaks were typically observed corresponding to different spatial modes. The ratio of distance between two peaks of matching (e.g. fundamental) mode to the full width at half maximum gives the cavity finesse. Note these representative transmission data do not come from the same cavity as the subsequent amplification measurements.

and polished to a thickness of 50 μm and afterwards optically "superpolished" with a pulsed laser at 213 nm and 24 μJ pulse power under oxygen atmosphere. This achieved a very high surface smoothness of R_a = 0.4 nm, in an attempt to eliminate scattering losses from the surface.

In order to investigate NV^- lasing, this diamond was placed inside an open, mechanically tunable fibre cavity [31], consisting of a concave fibre end mirror and a flat mirror substrate, forming a stable semiconcave cavity as illustrated in Figure 1(a). The curvature radius of the fibre tip mirror was around 170 μm. This imposes an upper limit on the stable cavity length, but the high refractive index of diamond means that placing the sample in the cavity increases the effective maximum cavity length. This ensures that a stable cavity mode can be formed while maintaining a safe separation between the fibre tip and the diamond sample. The fibre was mounted on a piezo (Noliac shear piezo stack NAC2402-H3.4 for the amplification study presented here) to allow fine and rapid control of the cavity length. Both cavity mirrors were coated with the same distributed Bragg reflector (DBR) coating (Laseroptik GmbH, Germany) designed to have two stopbands, one at 633 nm and the other one at 740 nm. The cavity was mechanically designed to achieve passive stability sufficient for this study.

Green off-resonant pump light at 532 nm (Lighthouse Photonics) and seed red light at 721 nm (MSquared SOLSTIS) were both delivered into the fibre cavity through the fibre-mirror end. At 532 nm, the dielectric DBR coating transmits roughly 60% of the incoming light generating a poor cavity mode. This makes it possible to achieve high pump laser powers at the sample, regardless of cavity tuning. A red laser wavelength at 721 nm was chosen over a 740-nm laser, where the cavity reflectively is at a maximum, because a lower reflectively will produce a lower finesse cavity which is less susceptible to noise and easier to handle without electronic stabilisation. The designed finesse for the cavity around 721 nm is around 40,000. Experimentally measured cavity finesse was around 100 times lower, limited by many factors such as light absorption in and surface scattering off the diamond sample. The light exiting the cavity through the macroscopic mirror substrate was collected and sent for analysis to a spectrometer (ACTON/Princeton Instruments SpectraPro 2500i). Before detection, the green pump light was blocked with a 532-nm notch filter. In the absence of an active feedback mechanism, we captured the cavity resonance for the 721-nm laser by applying a triangle-ramped voltage with 1 Hz frequency to the piezo that controls the cavity length. The shear piezo travel range was sufficient to cross multiple cavity resonances; Figure 1(b) shows an example of the upward ramp across two resonances, but in the diamond-loaded cavity for the amplification measurements the full range covered in one half of the triangular wave was about 10. The spectrometer camera integration time was set to 10 s so that all photons arriving at the detector from the cavity resonances crossed (naively about 200 in total) were captured for better signal-to-noise ratio. Naively, the cavity length was within the range of around

50–54 µm, during the cavity ramp. The spectrometer camera and cavity ramp were time synchronised.

3 Experimental results

Typical spectra under different pumping conditions are displayed in Figure 2. The solid green trace was recorded for 532-nm off-resonant green pumping alone, whereas the dashed orange trace was recorded for the same green pumping intensity with the red laser added at 721 nm. In essence, both spectra show a broad spontaneous emission background from the NV phonon sideband that is modulated with a period of 2.11 nm. This modulation is due to the diamond sample, and the period matches what is expected from its thickness of 50 µm. Clearly, the spectra have very similar broad backgrounds, but the orange trace with the red laser added shows the 721-nm resonant cavity mode appearing above the NV phonon sideband.

In order to see the difference between the two traces, we subtract the orange trace (red plus green lasers) from the green trace (green laser alone). Comparing the resulting trace with a spectrum of the red 721-nm laser alone, shown in red on the same plot, allows us to observe the impact of the additional red laser on NV centres excited by the green laser. The first impact of the red laser on the excited NV centres is a slight reduction in the background fluorescence (Figure 2(ii)). Secondly, the red laser peak has an increased intensity indicating an amplification of the power in the 721-nm cavity mode (Figure 2(iii)). As expected, the red trace is flat in the range between 711 and 721 nm of the spectrum since under red pumping alone, no noticeable spontaneously emission photons from NV centres are detected. In contrast to the amplified laser peak, the purple trace shows a negative background with a clear modulation contrast reminiscent of the large modulated background in part (i). This indicates that when both lasers are present, the spontaneous background is suppressed whilst the red laser is being amplified.

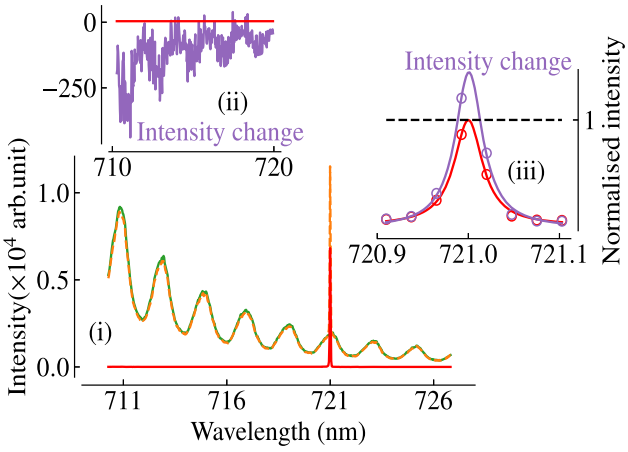

Figure 2: Typical experimental spectra obtained in cavity transmission. The green, orange, and red traces in (i) were obtained with green laser only, with the green plus red laser, and with the red laser only present, respectively. The modulation pattern with a period of about 2.11 nm in (i) is due to the weak cavity modes formed inside the diamond crystal itself. Subtracting the green trace from the orange trace yields the purple trace in (ii) and the data points shown in (iii) as purple circles (annotated as the intensity change in both figures). The red trace in (ii) is the spectrum with only the red laser near 721 nm present shown in (i). The red and purple lines shown in (iii) is the Lorentzian fit to the data points shown in respective colours. In the trace with green plus red laser present, a slight decrease in the spontaneous emission occurs compared to the green laser only trace, which is apparent in (ii). Amplification of the red laser is apparent at the cavity mode resonant with the red laser in (iii).

We vary the excitation power and observe the output of the cavity mode in a systematic fashion. In a first set of measurements, we keep the red power around 67 µW, and we vary the green pump power roughly between 1 and 150 mW. Both numbers refer to the input power into the cavity fibre. At each green pump power, we obtain a series of spectra as in Figure 2(i). We then compare the corresponding purple and red traces (Figure 2(iii)) to extract the amplification factor for the resonant laser in a quantitative way. The dimensionless ratio of the two, f_{amp}, obtained by the numerical summation of the data points, is a measure of the amplification of the red laser light transmitting through the cavity under green pumping. Figure 3(i) displays the resulting amplification factor f_{amp} as a function of the green pump power. Clearly, we see an amplification factor above one that monotonically increases over the power range plotted here (except the last data point). However, the trend shows a strong saturation behaviour, and the further increase in amplification for higher green pump power is only weak. In addition, we extract a quantitative measure for the effect of the red laser on the spontaneous emission from the NV centres. We therefore take the orange curve in Figure 2 (green plus red laser) and subtract the red curve (red laser only) from it. For the resulting trace (not displayed in Figure 2), we numerically sum the data points for the range shown in Figure 2(ii). The ratio f_{sp} of this integrated intensity to the integrated intensity of the corresponding wavelength region in the green spectrum of Figure 2(i) (green laser only) gives a quantitative measure for the effect of the red laser on the NV spontaneous emission.

Interestingly, when plotting f_{sp} as a function of green pump power (Figure 3(ii)), we observe an initial decrease in spontaneous emission as expected in the presence of

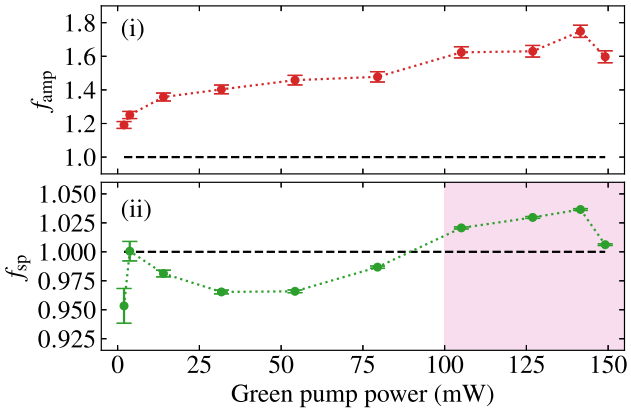

Figure 3: Amplification and spontaneous-emission factor as a function of green pump power. Error bars shown are one standard deviation range obtained by propagating the shot noise in spectrometer counts for each pump powers. (i) f_{amp} was extracted from raw data like the ones displayed in Figure 2 and measures the amplification of the red laser upon off-resonant pumping of nitrogen-vacancy (NV) centres. (ii) f_{sp} measures the influence of the red laser on the spontaneous emission of the NV centres and was obtained by integration of the background signals in the wavelength region of the inset of Figure 2 (ii). The black dotted lines indicate the reference line at unity, which corresponds to no difference in the output signal between the different pumping schemes.

stimulated emission. But as we increase the green pump power beyond 50 mW, the trend reverses, and somewhat surprisingly, we see more NV centre spontaneous emission in the presence of the resonant laser than without it (the shaded magenta region in Figure 3(ii)). Interestingly, f_{sp} seems to follow the behaviour of the corresponding f_{amp} in the shaded region. Both the strong saturation of the amplification factor, f_{amp}, and the "reversing" behaviour in the spontaneous emission factor, f_{sp}, raise questions about the underlying physical mechanism. In the following section, we therefore present a qualitative model that sheds some light on the physics going on in our diamond-cavity system.

This measurement of amplification as a function of green pump power was repeated for a systematic range of the red probe laser powers. The observed effect of the red laser power on f_{amp} is summarised in Figure 4. As the red power increases from around 1 to around 47 mW, amplification gets increasingly suppressed, as witnessed by the fact that f_{amp} saturates much more rapidly and essentially stays flat around one for the highest red powers. In order to quantify this effect, in Figure 4(b), we plot f_{amp} as a function of red power for fixed green pump powers (corresponding to the marked vertical slices through the data in Figure 4(a)). These data fit well with an inverse square law as demonstrated by the fit curves displayed alongside the data points.

Finally, we would like to point out that in different iterations of our experiment (with slight changes to the set-up and cavity parameters), we have consistently observed amplification factors up to a maximum of ~3 and similar reversing trends in the spontaneous emission signal that also include the peculiar increase in f_{sp} above 1 for higher green pump powers. In addition to this, we have observed reduction in the amplification factor f_{amp} below one in some of our measurements with high red laser power. This is also apparent in some of the data points, particularly for low green pump powers and high red laser power in Figure 4(A).

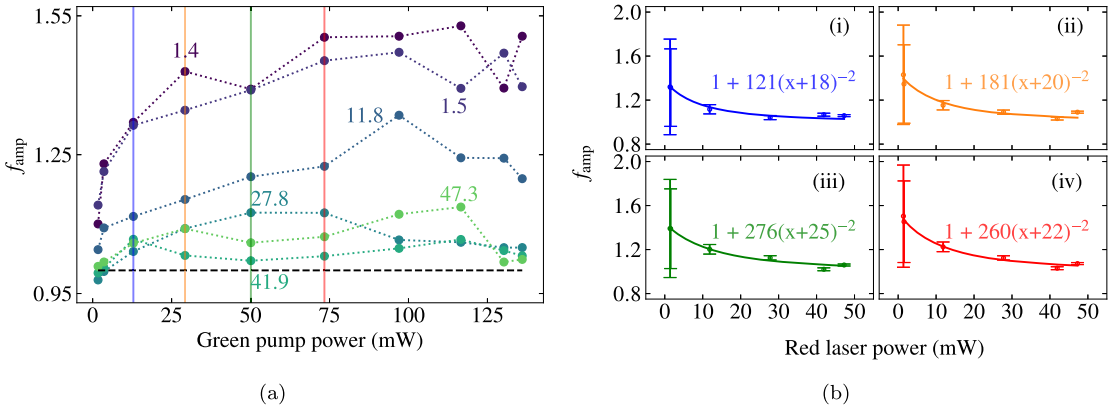

Figure 4: Dependence of f_{amp} on red power. (a) f_{amp} as a function of green pump power for different red powers. Red laser power in mW, corresponding to each curve, is annotated in respective colours. (b) Line cuts through (a) give f_{amp} as a function of red laser power for fixed green pump power. The blue, orange, green, and red colours in (i), (ii), (iii), and (iv) correspond to green pump powers of ~12.9 mW, ~29.2 mW, ~50.1 mW, and ~73.4 mW, respectively. The solid curves with respective colours are from the fit functions annotated in each figures. For clarity, error bars, which are obtained in the same manner as Figure 3, are shown only in (b).

4 A qualitative model based on stimulated emission and charge state switching

In this section, we theoretically model an ideal amplification experiment taking into account the photoinduced charge interconversion between NV^- and NV^0, as well as the stimulated emission from these charge states. The results from the theoretical modelling allow us to qualitatively interpret the experimental results of the previous section.

4.1 Model

We consider an ideal cavity on resonance with the red laser at 721 nm in the fundamental (Gaussian) mode. For ease of calculation, we assume a flat-top approximation and a cylindrical volume of the cavity, with the radius of the Gaussian spot size on the macroscopic mirror as the base radius. We further assume that the cavity is fully filled with the diamond sample. The effective cavity volume determines the number of NV centres contributing to the dynamics and the laser amplification. It further sets the stimulating intracavity power/intensity of the red laser by scaling the power that we provide at the fibre input by the effective finesse of the cavity.

In order to model the NV centres in our cavity, we first consider a single NV centre and capture its internal dynamics including charge state switching. We then simply scale the population fractions with the total number of NV centres inside the cavity volume to obtain the ensemble effect. A review of the NV centre charge state switching dynamics is given in Appendix A, and the resulting level scheme and transitions are depicted in Figure 5. We can then write down the rate equations based on the level scheme in Figure 5.

$$\frac{\mathrm{d}p_{|1\rangle}}{\mathrm{d}t} = -\left(\frac{I_g\sigma_g}{h\nu_g}+\frac{I_r\sigma_r}{h\nu_r}\right)p_{|1\rangle} + r_{31}p_{|3\rangle} + \frac{I_r\sigma_{se}}{h\nu_r}p_{|3\rangle} + r_{51}p_{|5\rangle} + \frac{1}{2}\left(\frac{I_g\sigma_R^g}{h\nu_g}+\frac{I_r\sigma_R^r}{h\nu_r}\right)p_{|7\rangle}, \tag{1}$$

$$\frac{\mathrm{d}p_{|2\rangle}}{\mathrm{d}t} = -\left(\frac{I_g\sigma_g}{h\nu_g}+\frac{I_r\sigma_r}{h\nu_r}\right)p_{|2\rangle} + r_{42}p_{|4\rangle} + \frac{I_r\sigma_{se}}{h\nu_r}p_{|4\rangle} + r_{52}p_{|5\rangle} + \frac{1}{2}\left(\frac{I_g\sigma_R^g}{h\nu_g}+\frac{I_r\sigma_R^r}{h\nu_r}\right)p_{|7\rangle}, \tag{2}$$

$$\frac{\mathrm{d}p_{|3\rangle}}{\mathrm{d}t} = -\left(r_{31}+r_{35}+\frac{I_g\sigma_I^g}{h\nu_g}+\frac{I_r\sigma_I^r}{h\nu_r}\right)p_{|3\rangle} + \left(\frac{I_g\sigma_g}{h\nu_g}+\frac{I_r\sigma_r}{h\nu_r}\right)p_{|1\rangle}, \tag{3}$$

$$\frac{\mathrm{d}p_{|4\rangle}}{\mathrm{d}t} = -\left(r_{42}+r_{45}+\frac{I_g\sigma_I^g}{h\nu_g}+\frac{I_r\sigma_I^r}{h\nu_r}\right)p_{|4\rangle} + \left(\frac{I_g\sigma_g}{h\nu_g}+\frac{I_r\sigma_r}{h\nu_r}\right)p_{|2\rangle}, \tag{4}$$

$$\frac{\mathrm{d}p_{|5\rangle}}{\mathrm{d}t} = -\left(r_{52}+r_{51}+\frac{I_r\sigma_I^s}{h\nu_r}\right)p_{|5\rangle} + r_{35}p_{|3\rangle} + r_{45}p_{|4\rangle}, \tag{5}$$

$$\frac{\mathrm{d}p_{|6\rangle}}{\mathrm{d}t} = -\frac{I_g(\xi\sigma_g)}{h\nu_g}p_{|6\rangle} + \left(r_{76}+\frac{I_r(\eta\sigma_{se})}{h\nu_r}\right)p_{|7\rangle} + \frac{I_r\sigma_I^s}{h\nu_r}p_{|5\rangle} + \left(\frac{I_g\sigma_I^g}{h\nu_g}+\frac{I_r(\sigma_I^r)}{h\nu_r}\right)\left(p_{|3\rangle}+p_{|4\rangle}\right), \tag{6}$$

$$\frac{\mathrm{d}p_{|7\rangle}}{\mathrm{d}t} = -\left(r_{76}+\frac{I_r(\eta\sigma_{se})}{h\nu_r}\right)p_{|7\rangle} - \left(\frac{I_g\sigma_R^g}{h\nu_g}+\frac{I_r\sigma_R^r}{h\nu_r}\right)p_{|7\rangle} + \frac{I_g(\xi\sigma_g)}{h\nu_g}p_{|6\rangle}. \tag{7}$$

Here, $p_{|j\rangle}$ is the population fraction of a single NV centre on the level $|j\rangle$. Thus, $\sum_{j=1}^{7}p_{|j\rangle}=1$. Since the decay from the phonon levels of the ground state is expected to be very fast, we neglect any stimulated absorption from these phonon levels back to the excited states. From the model, we obtain the steady-state population fractions of each of the seven levels, denoted by p_i with $i = 1, \ldots, 7$. The spontaneous and stimulated emission intensity of the NV centres can then be calculated from the steady-state populations in the excited states of both the NV^- charge state ($p_{|-\rangle}=p_{|3\rangle}+p_{|4\rangle}$) and the NV^0 charge state ($p_{|0\rangle}=p_{|7\rangle}$).

In our qualitative model, we make the following assumptions for simplicity. Firstly, whilst the coupling between each NV centre in the diamond and the cavity mode really is different [33], we assume every NV centre in the diamond to have the same coupling for simplicity of calculation and in order to extract the essential physics. This model also neglects possible dipole–dipole interactions and coherent collective effects [34], which is reasonable given the typical cavity decay rates and the NV density in our system. In addition, since we are using high-intensity fields, we neglect the single photon ionisation process that has been observed for low-power off-resonant excitation [35]. We also do not consider the spin dependence on ionisation transitions directly from excited states that has recently been reported for nanodiamond NV ensembles [23] as it is not necessary in order to capture the important physics and trends observed in the data. However, an indirect spin dependence is included intrinsically on the ionisation through the spin-dependent transition to the singlet states [36] and also through the ionisation from the singlet state due to the NIR wavelength [22]. Furthermore, emission of the NV^0 that may then be subsequently captured by surrounding NV^- centres has not been considered in this model. In dense NV samples, this effect will reduce the effective contribution of NV^0 in the emitted signal; however, we expect this effect to be small. Lastly,

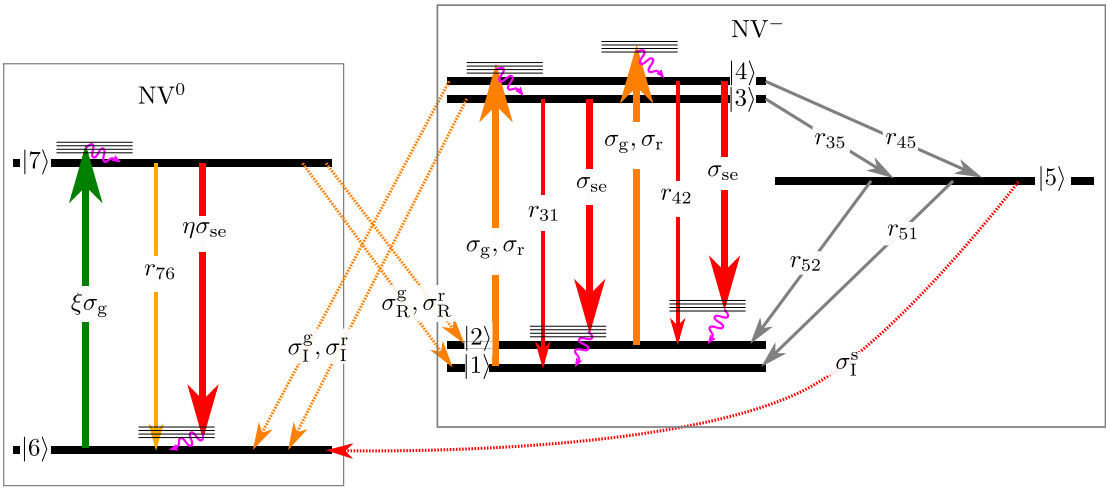

Figure 5: Nitrogen-vacancy (NV) centre model for explaining amplification. Levels 1–5 belong to NV^- and six and seven belong to NV^0. In the NV^-, 1 and 2 respectively represent $m_s = 0$ and $m_s = \pm 1$, respectively, of the ground state, and 3 and 4 respectively represent $m_s = 0$ and $m_s = \pm 1$, respectively, of the excited state. Five represent the singlet level of the NV^- centre. In the case of NV^0, it has only the ground state (6) and excited state (7). The orange arrows represent transitions due to both green and red wavelengths. The solid orange line represents the pumping rate, whereas the dotted one represents the ionisation and recombination transitions. The thin and thick solid red arrows represent spontaneous and stimulated transitions. The grey arrows represent intersystem crossing (ISC) transitions, and curly magenta arrows represent phonon decays. The green arrow represents the pumping rate of NV^0 by the green wavelength. The transition rates of each transition are shown on each corresponding arrows.

we do not consider any change in the cavity conditions that modify the input light into the cavity and thereby change the intracavity field as well as the cavity transmission for simplicity.

Both charge states can contribute to the stimulated emission signal since both charge states have a broad phonon sideband with a significant amplitude at 721 nm. The amplification factor, f_{amp}, is a ratio of the total intracavity power at 721 nm to the intracavity power of the seed laser. Assuming stimulated emission of the two charge states of NV centres as the additional contribution to the intracavity power at 721 nm, other than the external seed laser at 721 nm, the f_{amp} can be written as

$$f_{amp} = 1 + \left(p_{|-\rangle} + \eta p_{|0\rangle}\right) F \sigma_{se} \rho_{NV} l. \tag{8}$$

Here, σ_{se} is the stimulated emission cross section of the NV centre in the negative charge state. η represents the ratio of stimulated emission cross sections of NV^0 to NV^-. ρ_{NV} is the density of the NV centres in the diamond sample, and l is the cavity length, which in our simplified model, we assume to be the thickness of the sample. F denotes the ratio of the intracavity resonant (red) laser power and the input power at the fibre input, which can be approximated as finesse/π. It is important to note that the assumption leading to this equation's simplicity is that the change in spontaneous emission when adding the red seed laser is small compared with the stimulated emission cross section, which is valid for the seed intensities used in this paper. We further simplify by neglecting the fact that the stimulated emission can happen in both directions of the cavity, and we are only collecting photons in the transmission of the seed laser. Qualitatively, this makes no difference.

Next, we can obtain the spontaneous emission factor, f_{sp}, by comparing the number of photons spontaneously emitted under green plus red pumping with that emitted under green pumping only. We include both charge states and write f_{sp} as

$$f_{sp} = \frac{p_{|-\rangle} + \beta p_{|0\rangle}}{p'_{|-\rangle} + \beta p'_{|0\rangle}}. \tag{9}$$

The prime (′) marks the population fractions under green pumping only, and β is the ratio of the spontaneous emission rate of NV^0 to NV^-. We neglect the emission from the NV^0 when there is only red laser present, since the red laser cannot excite this centre in our model.

4.2 Numerical results

To model the NV centre, we have used the parameters shown in Table 1. These were obtained from the literature, specifically for HPHT type 1b bulk diamond where possible. The choice for some parameters was complicated by considerable variation across previous publications. For example, we consider a comparatively high value for a

Table 1: Parameters used for the theoretical estimations. The transition rates are the average of the values from the study by Tetienne et al. [37]. σ_g is the absorption cross sections of NV^- for green wavelengths.

Parameter	Value	Reference
$r_{31} = r_{42}$	63.93 μs^{-1}	[37]
r_{35}	7.93 μs^{-1}	[37]
r_{45}	53.25 μs^{-1}	[37]
r_{51}	0.98 μs^{-1}	[37]
r_{52}	0.72 μs^{-1}	[37]
r_{76}	$0.74 \times r_{31}$	[22]
σ_g	3.1×10^{-21} m^2	[38]
σ_I^g	$0.037 \times \sigma_g$	[22]
σ_R^g	$0.08 \times \sigma_g$	[22]
σ_I^r	$0.071 \times \sigma_{se}$	[22]
σ_R^r	$0.22 \times \sigma_{se}$	[22]
σ_I^s	$0.0215 \times \sigma_{se}$	[22]

NV, nitrogen-vacancy.

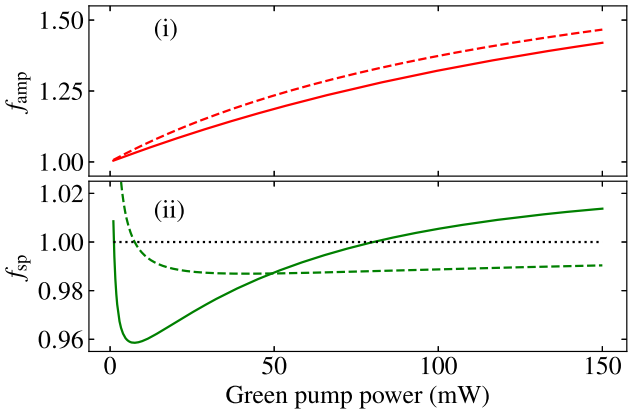

Figure 6: f_{amp} and f_{sp} from the qualitative model as a function of green pump power in (i) and (ii), respectively. The solid curves correspond to the case with charge state switching, and the dashed curves correspond to without charge state switching with only NV^-. The black dotted line is the reference line at factor 1.

singlet-state lifetime based on the study by Tetienne et al. [37] although lower values are also reported in the literature [1]. The choice of a somewhat longer singlet-state lifetime could be justified potentially through the presence of NV centre transitions to dark states, e.g. through excited-state absorption, which is not separately considered in our model. Also, in our experiment, we do not observe any saturation of the spontaneous emission from the NV centres, and so we consider a lower value of the absorption cross section for the green available in the literature from Wee et al. [38] and Dumeige et al. [39]. The ratio of the ionisation or recombination cross section to the absorption cross section (stimulated emission cross section) for the green wavelength (red seed wavelength) was considered from the study by Hacquebard and Childress [22]. The green wavelength in that study is close to the one in the present study. Although the red wavelength considered in the study by Hacquebard and Childress [22] is different, we consider these experimental values for the present study, assuming they do not differ very much.

The stimulated emission cross section $\sigma_{se} \sim 3.22 \times 10^{-21}$ m^2 for our sample is obtained in a similar fashion to the study by Fraczek et al. [29], but considering only the NV^- centres (see Appendix B). The value we obtain for our system is comparable to the values obtained in the literature previously [19, 29, 30]. Near our working wavelength of 721 nm, the study by Fraczek et al. [29] specifies a ratio between the stimulated emission cross section of NV^- and NV^0 of slightly higher than 3. Hence, we assume $\eta_{se} = \frac{1}{3}$ in our model.

Figure 6 shows plots of f_{amp} and f_{sp}, as defined in Eqs. (8) and (9), respectively, as a function of green pump power in Figure 6. Both the calculated amplification factor f_{amp} and the spontaneous emission factor f_{sp} qualitatively match the behaviour observed in our experiments. To achieve this, we assumed the free parameters $F \sim 500/\pi$, $\xi = 0.66$, $\sigma_r = 2 \times 10^{-23}$ m^2, and the radius of the cavity mode waist as 5 μm.

Given the design finesse of around 40,000 and the surface roughness and thickness of the diamond sample, the value of F seems reasonable as the finesse assumed is within the experimental uncertainties of the finesse we typically observe in our diamond-loaded cavity. The parameter ξ is the ratio of excitation efficiency of the NV to NV^-. This value is not consistent in the literature and ranges from 0.33 to 1.8 [22, 23, 35, 40]. The value used here lies within this range and is therefore reasonable. The absorption cross section for the red wavelength is expected to be smaller than that for green wavelength [20]. Though the value we used in the present study is roughly an order of magnitude higher than the absorption cross section of a lower red wavelength [20], it is still roughly two orders of magnitude lower than the absorption cross section for the green wavelength. The radius of the empty cavity mode waist can be estimated to be around 4.22 μm corresponding to a cavity length of 50 μm and the radius of curvature of the fibre mirror in our cavity. The cavity mode is expected to be slightly enlarged in the diamond-loaded cavity [33]. A precise estimation of this value requires careful consideration of diamond and air layers inside the cavity. Since we are examining the model qualitatively, the radius of the cavity mode waist used is justifiable.

In order to understand the underlying physics, we also plot the calculated relevant populations of NV^- and NV^0 in Figure 7. This graph clearly reveals the influence of ionisation on the observed cavity output. At any green pump power, the

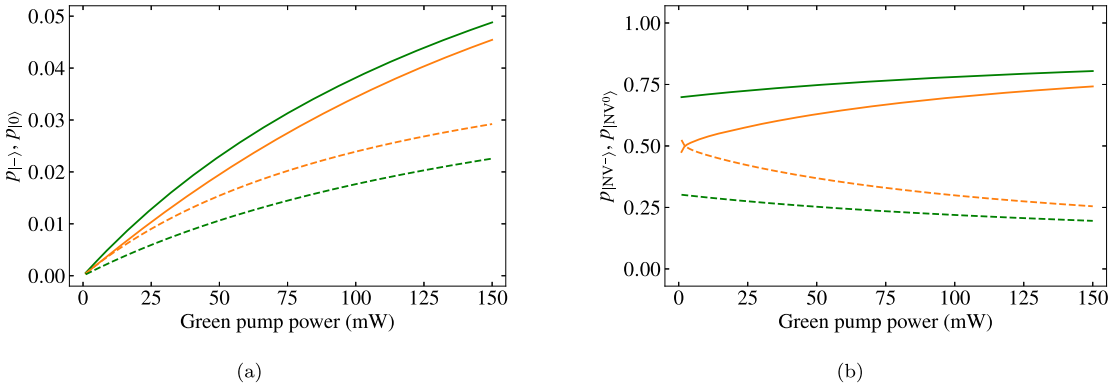

Figure 7: (a) $p_{|-\rangle}$ and $p_{|0\rangle}$ as a function green pump power. Green and orange colours represent green alone pumping and green plus red pumping, respectively. The solid and dashed lines correspond to NV^- and NV^0, respectively. For green plus red pumping, stimulated emission of NV^- and NV^0 is considered. However, for green alone pumping, we neglect the possibility of stimulated emission from any of the charge states considering the fact that the spontaneous emission from these charge states into the cavity is not stimulating the emission as we do not see any trace of it in our experiment. (b) Total fraction of NV^- and NV^0. The plot styles follow the same as (a).

population in NV^- dominates over the NV^0 population. The red laser enhances the ionisation towards NV^0 as is evident from the fact that the orange dashed line representing the NV^0 population under green plus red pumping lies significantly higher than the green dashed line representing green pumping only. Similarly, the solid orange line representing the NV^- population under green plus red pumping lies below the solid green line for green pump only. Furthermore, in our model, the excited-state population of each charge state that determines the gain is much smaller than the total population of the respective charge state. This is due to the significant population in the ground state of both charge states and also in the singlet state for the NV^- centre.

Our model is also able to qualitatively capture the observed dependence of the amplification factor f_{amp} on the red laser power (see Figure 3). Figure 8 displays the calculated f_{amp} as a function of green pump power for different red pump powers, alongside the corresponding line cuts at constant green pump power, similar to the experimental curves in Figure 3. We observe a similar overall trend in f_{amp} as compared to experiments. In particular, we also observe the quadratic decrease of f_{amp} as a function of red laser power for a fixed green pump power.

5 Discussion

In the light of the model presented in the previous section, we interpret the amplification at 721 nm observed in the experiment to be due to stimulated emission from both the charge states of NV centres. In the experiments, owing to

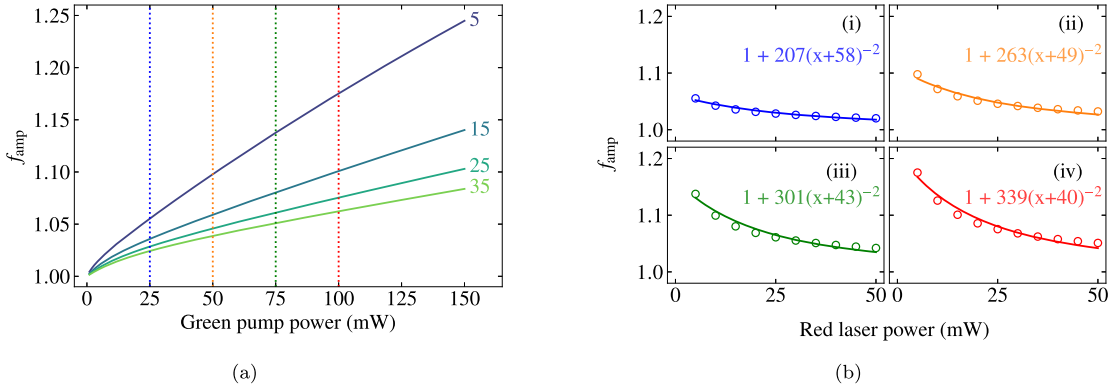

Figure 8: Change in amplification factors calculated from the theoretical model as a function of red laser power. The red laser power in mW is annotated for each cure in their respective colours. (b) The amplification factors in the dotted lines drawn in (a) as a function of red laser power. The blue, orange, green, and red circles in (i), (ii), (iii), and (iv) are the amplification factors corresponding to the green pump powers 25 mW, 50 mW, 75 mW, and 100 mW, respectively, where the dotted lines are drawn in (a) with respective colours. The solid curves with respective colours are the fit functions annotated in each figure.

the cavity length tuning, the red seed wavelength can excite both fundamental Gaussian as well as higher order Hermite–Gaussian spatial modes in the cavity. Similarly, the emission of NV centres can be in the fundamental Gaussian as well as into the higher order transverse modes of the cavity. Since the coupling into the cavity mode and the spatial distribution of the cavity mode varies depending on the order of the mode [33], the amplification factor due to stimulated emission is also expected to have different values for the different cavity modes. The maximum amplification is expected to happen in the fundamental mode of the cavity. Therefore, the actual amplification factor for the fundamental mode is likely to be higher than the averaged amplification factor observed in our experiments.

The observed drop of f_{sp} below one and then the rise of this factor above one for increasing pump powers are a significant focus of simulation. For the spontaneous emission dynamics in this model, photons emitted from the NV^0 charge state are playing a central role. At low green pump powers, the number of spontaneous photons is reduced when the red seed light is added. Since the model without the ionisation shows the same trend, the reduction in spontaneous emission can be attributed mainly to the stimulated emission. As a result, f_{sp} reduces for small pump powers (evident both in the simulated and measured data). As the green power increases, however, eventually spontaneous emission from NV^0 non-negligibly contributes to the fluorescence signal. For higher green pump powers, f_{sp} even increases above 1. In the absence of ionisation, the stimulated emission process should simply deplete the excited state, and the maximum f_{sp} would be 1. We therefore interpret the observed characteristic trend in f_{sp} accompanying the measured f_{amp} for higher green pump powers comes from both the stimulated emission of NV^- centres and charge state switching of these centres.

It should be highlighted that we have considered values here that come from diamond samples similar to those used in this study. A number of parameters and process within the model can be modified whilst still capturing qualitatively similar results as our experiment. Further detailed studies are required to examine the exactness of the parameters and the processes.

The minimum value for the f_{amp} for the model presented here is one and thus cannot account for the negative amplifications that we mentioned in the experimental results. Such cases can be attributed to additional mechanisms such as excited state absorption and photothermal/heating effects on the fibre.

6 Conclusion

We have presented experimental data showing amplification of red laser light in an open fibre cavity filled with highly NV-doped diamond. The amplification increases monotonically with green pump power. Based on our qualitative model of the underlying NV colour centre dynamics, we attribute the amplification to stimulated emission from NV centres. The observed effects of reduced spontaneous emission at lower pump powers and increased spontaneous emission at high powers were on the order of a few percentage. This trend was qualitatively reproduced in our model, including stimulated emission and charge state switching of NV centres. The observed effect is thus interpreted to arise from the fact that a fraction of the stimulated and spontaneous photons observed in the experiment (especially at higher green pump powers) is coming from the neutral charge state of the NV centre as well.

The relative amplification factors indicate that considerable stimulated emission occurs in the cavity; however, a strong absolute signal was not observed owing to cavity loss channels other than the mirror transmissions, in particular owing to the remaining absorption in the diamond material arising from either the NV centres themselves or other internal defects. For the realisation of an NV laser in the future, this poses the challenges of reducing the remaining strong absorption due to other structural or nitrogen-related defects in highly NV-doped diamond and highlights the importance of a stable charge state. We conclude that a majority of the currently commercially available type 1b diamond shows absorption in the red, amplified through the multiple passes of a cavity, which prevents active standalone lasing in fibre cavities. Having said that, much work remains to be done on exploring the physics and reducing the material loss channels, such as absorption and birefringence of highly NV-doped diamond for cavity and laser applications. This will involve substantial materials engineering including a detailed understanding of the nitrogen defects, structural defects, absorption from ground and excited states as well as charge donors and acceptors in the diamond crystal.

Acknowledgements: Sarath Raman Nair acknowledges that this work was done while holding International Macquarie University Research Excellence Scholarship (iMQRES) (allocation number 2014108) and also acknowledges EQUS centre collaboration award. Lachlan Rogers is the recipient of an Australian Research Council Discovery Early Career Award (project number DE170101371). This work was supported by

Australian Research Council Centre of Excellence for Engineered Quantum Systems (CE170100009). Jan Jeske acknowledges funding from the German Federal Ministry for Education and Research Bundesministerium für Bildung und Forschung (BMBF) under grant number 13XP5063. Andrew D. Greentree acknowledges Australian Research Council under the Future Fellowship (FT160100357).

Author contribution: J.J., A.D.G., T.V., X.V., and S.R. conceived the initial ideas about the experiments. J.J., X.V., S.R., L.J.R., and T.V. planned the experiments. H.A., T.O., T.Y., and J.J. prepared and processed the diamond sample. S.R. and L.J.R. built the experiments with contributions from X.V. S.R. took measurements and analysed the data with contributions from L.J.R. S.R. performed the theoretical modelling and simulations. S.R., T.V., L.J.R., R.P.R., and J.J. interpreted the results. S.R., T.V., L.J.R., and R.P.R. wrote the manuscript with varying contributions from all authors. T.V. supervised the project.

Research funding: Sarath Raman Nair acknowledges that this work was done while holding International Macquarie University Research Excellence Scholarship (iMQRES) (allocation number 2014108) and also acknowledges EQUS centre collaboration award. Lachlan Rogers is the recipient of an Australian Research Council Discovery Early Career Award (project number DE170101371). This work was supported by Australian Research Council Centre of Excellence for Engineered Quantum Systems (CE170100009). Jan Jeske acknowledges funding from the German Federal Ministry for Education and Research Bundesministerium für Bildung und Forschung (BMBF) under grant number 13XP5063. Andrew D. Greentree acknowledges Australian Research Council under the Future Fellowship (FT160100357). Takashi Yatsui acknowledges funding from JSPS KAKENHI (No. JP18H01470) and the Asahi Glass Foundation.

Conflict of interest statement: The authors declare no conflicts of interest regarding this article.

Appendix A: Charge state switching dynamics

To convert between the two charge states, we need to examine both the ionisation process from NV^- to NV^0 and the recombination process from NV^0 to NV^- as depicted in Figure 9. The charge state switching dynamics in NV centres is a complex problem that is still being studied actively in the community. One problem is that the dynamics depend strongly on the properties of the diamond; in particular, the density of the NV centres, the surrounding singlet nitrogen charge donors, and the impact of surface charge acceptors all play a significant role, varying dramatically between diamond samples. Including the properties of the singlet nitrogen in the diamond lattice is essential for understanding the dynamics as they are the main defect responsible for supplying the NV centres with an additional charge [41]. In the dark, the charge state of individual NV centres depends on the separation distance between the NV centre and the singlet nitrogen. For small N to NV separations (~5 nm), an electron will tunnel from the singlet nitrogen to the NV centre to produce an $NV^- - N^+$ pair [35]. For these diamonds, the conversion of the NV^- centre into the NV^0 charge state can occur via a single-photon process. The NV^- centre must first be excited into the excited state where the electron can then tunnel back to the singlet nitrogen, leaving the NV centre converted into the NV^0 charge state. As mentioned by Manson *et al.*, tunnelling from the excited state of the NV^-, $^3E(e^3a)$ state to the ground state of the NV^0, $^2E(a^2e)$ is unlikely to occur as this would involve a two-electron transition. It is therefore more likely that the NV^- excited state, $^3E(e^3a)$ tunnels directly to the metastable $^4A_2(e^2a)$ quartet level before decaying nonradiatively to the NV^0 ground state, $^2E(a^2e)$. Additionally, it is also possible that tunnelling occurs through the NV^- metastable, $^1E_1(a^2e^2)$ state to the ground state of NV^0, $^2E(a^2e)$. It is clear that the specific details of the tunnelling transitions require further experimental and theoretical consideration. For larger NV–N separations as well as for higher intensity excitation, ionisation from NV^- to NV^0 occurs through a two-photon process. First, the NV^- centre must be excited, and then, subsequently, a second electron is stripped from the NV^- complex. This second ionisation step occurs either from the excited $^3E(e^3a)$ state or from the $^1E_1(a^2e^2)$ state of the NV^- [22]. Using similar arguments as above, it is likely that this will produce NV^0 centres in the metastable $^4A_2(e^2a)$ quartet level, or ground $^2E(a^2e)$ state, respectively. Interestingly, both the 532-nm excitation laser and 721-nm seed laser can induce both of these processes, the 721-nm seed laser only weakly excites the NV^- centre and more efficiently induces the second ionisation step. The result of this is that increasing the 721-nm field intensity leads to a stronger nonradiative transition to the NV^0 ground state. In addition, using 721-nm continous wave (CW) excitation alone, negligible fluorescence will be observed since the excitation cross section is small, and this laser preferentially populates the NV^0 charge state. The NV^0 charge state can then not be excited at this wavelength, resulting in no fluorescence signal.

The recombination process from NV^0 to NV^- can also occur through a tunnelling process or a two-photon process. The tunnelling process for close NV–N pairs as described above is caused by a singlet nitrogen providing the electron which is captured by the NV^0 in its $^2E(e^2a)$ ground state tunnelling to the NV^- in its $^3A_2(a^2e^2)$ ground

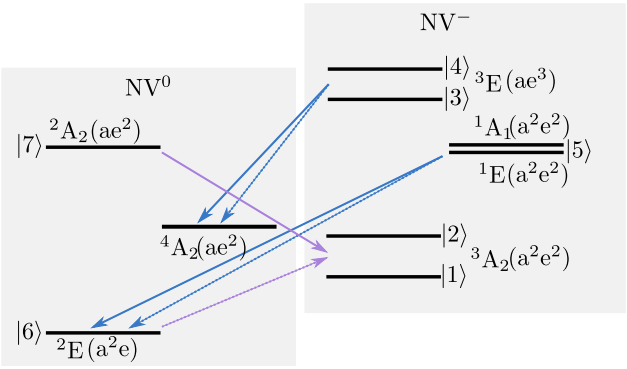

Figure 9: Electronic energy level scheme of the nitrogen-vacancy (NV) centre showing the ionisation and recombination processes that have been observed. Levels 1–5 belong to NV^- and 6 and 7 belong to NV^0 and have been labelled with their corresponding molecular symmetry assignments as well as their molecular electron orbital states. This picture shows that state 5 is in fact two distinct energy levels and there is also a spin quartet metastable state that plays a role in the ionisation dynamics. These states have been removed in Figure 4 as they do not significantly impact the rate equation description of the system. The blue arrows indicate ionisation pathways from the NV^- state to the NV^0 state, whereas the purple arrows indicate recombination pathways from NV^0 to NV^-. The dashed arrows indicate tunnelling processes that are mediated by a nearby single substitutional nitrogen acting as a charge donor to the NV centre. The solid lines are photon-mediated processes. At this stage, it is uncertain if all of these photon-mediated processes are intrinsic to the NV centre or are due to ionisation of nearby charge donors leading to a tunnelling process. It is unlikely that ionisation from the $^3E(ae^3)$ excited state of the NV^- occurs directly to the $^2E(a^2e)$ ground state of the NV^0 as this must involve a two-electron process. It is more likely that the transition occurs into the $^4A_2(ae^2)$ metastable state of the NV^0 centre before quickly and nonradiatively decaying into the ground state of the NV^0. In the rate equation models used to simulate this system, these two processes are approximately equivalent. It is important to note that there may be additional allowed pathways for ionisation such as from the $^3E(ae^3)$ excited state of the NV^- into the $^2A_2(ae^2)$ excited state of the NV^0 that we have not considered in this paper.

state. The two-photon process from NV^0 to NV^- occurs again by accepting a charge from a nearby charge donor. Firstly, a photon must excite the NV^0 into its $A_2(ae^2)$ excited state. Subsequently, a second electron can then be excited from the valence band, providing the additional electron required to turn the transition of the centre into the NV^-, $^3A_2(a^2e^2)$ ground state [42]. The second step of this process is considered to be mediated by charge donors in the diamond lattice. For typical diamonds that contain NV centres, this is dominated by the surrounding singlet nitrogen which can be ionised for energies from 1.7 to 2.2 eV [43, 44]. At the lower ionisation estimates, both the 532- and 721-nm fields can ionise the singlet substitutional nitrogen, leading to extra-free electrons producing NV^- centres. Interestingly, an increase in the recombination rate has been observed for under NIR illumination for ensembles of NVs in nanodiamonds at 785 nm [23] and for single NV centres in bulk at 766 nm [22]. Both of these wavelengths should not have enough energy to excite the singlet nitrogen; nevertheless, the recombination is still observed. For ensembles, the increase in red-induced recombination could be arising from an increased rate of ionisation of the surrounding NV^- centres in the diamond, producing free electrons for NV^0 recombination. However, for single NV centres, this effect should not be possible. This wavelength independency of the recombination raises questions over the exact processes involved in the charge state switching. It is possible therefore that the ionisation and recombination processes of the NV centres are not intrinsic to the NV centres but mediated by the broadband ionisation of donors and acceptors within the diamond lattice causing NV tunnelling rates to increase. If this is indeed the case, then it may still be possible to engineer diamond samples with stabilised NV^- centres that are less sensitive to the intense NIR fields required for some applications including the NV^- laser magnetometer.

Appendix B: Stimulated emission cross section

We estimate the stimulated emission of the NV centre in a similar way of the study by Fraczek et al. [29], but without specification to the charge state. For this, we obtain the spectrum of the NV centre normalised to the peak intensity, without any cavity for an arbitrary green pump power. This normalised spectrum is shown in Figure 10. The fit

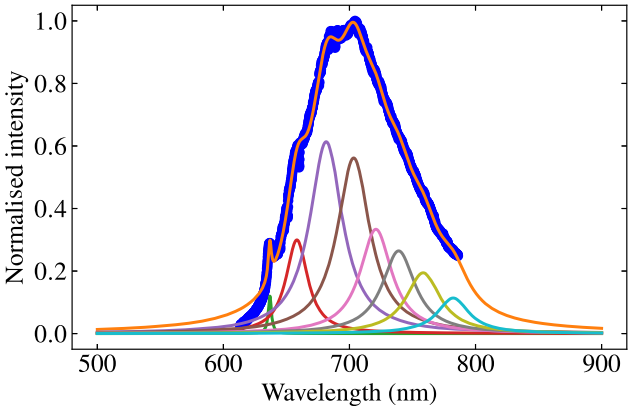

Figure 10: Spectrum of the nitrogen-vacancy (NV) centre from our sample by green wavelength pumping without any cavity mirrors. The blue dots are the experimentally obtained spectrum. The orange curve is the fit using a convolution of eight Lorentzian functions for the zero-phonon line (ZPL) and seven phonon levels. The individual Lorentzian functions are also shown. See the text for the details.

Table 2: Parameters obtained from the eight Lorentian fit functions of the spectrum.

Peak position	Amplitude	FWHM
636.9 nm	0.1	3 nm
658.3 nm	0.3	21 nm
681.5 nm	0.6	31.7 nm
703.4 nm	0.6	31.7 nm
721.0 nm	0.3	30.4 nm
739.0 nm	0.3	31.7 nm
758.5 nm	0.2	33.1 nm
782.3 nm	0.1	30.4 nm

FWHM, full width at half maximum.

parameters for the Lorentzian functions obtained from the fit are shown in Table 2. The fit shows that the peak position of one of the phonon levels is ~721 nm at the red wavelength. However, since the phonon levels are expected to have an extremely short lifetime, which induces very strong dephasing, we neglect any coherent transition from the phonon levels similar to the stimulated absorption case.

We calculate the stimulated emission cross section using the Füchtbauer–Ladenburg equation given as [29, 45, 46],

$$\sigma_{se}(\lambda) = \frac{1}{8\pi n^2 c\gamma} \frac{\lambda^5 I(\lambda)}{\int \lambda I(\lambda) d\lambda}. \quad (10)$$

Here, n is the refractive index of the diamond sample, c is the speed of light, γ is the spontaneous decay rate, λ is the wavelength, and $I(\lambda)$ is the intensity as a function of wavelength. We replace $\int \lambda I(\lambda) d\lambda$ in Eq. (10) with $\sum \lambda I(\lambda)\delta\lambda$. Then, we obtain $\sigma_{se}(\lambda)$ from the normalised spectrum (Figure 10), and the result is shown in Figure 11. To find the stimulated emission cross section, without specification to the charge state, we consider γ as r_{31}.

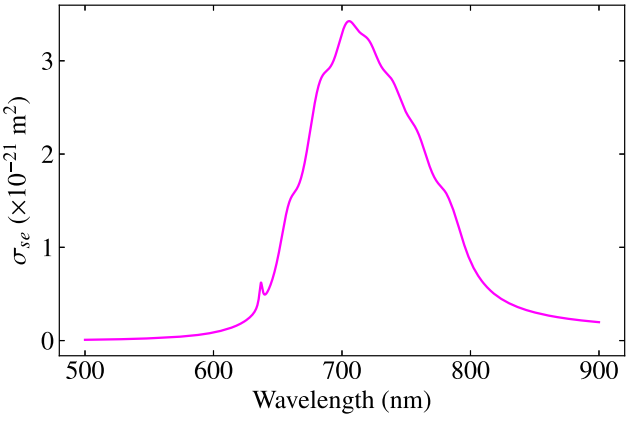

Figure 11: Spectrum of the nitrogen-vacancy (NV) centre from our sample by green wavelength pumping without any cavity mirrors. Stimulated emission of our sample as a function wavelength. At ~721 nm, $\sigma_{se} \sim 3.22 \times 10^{-21}$ m^{-2}.

References

[1] J. F. Barry, J. M. Schloss, E. Bauch, et al., "Sensitivity optimization for NV-diamond magnetometry," *Rev. Mod. Phys.*, vol. 92, no. 1, p. 015004, 2020.

[2] C. L. Degen, F. Reinhard, and P. Cappellaro, "Quantum sensing," *Rev. Mod. Phys.*, vol. 89, no. 3, p. 035002, 2017.

[3] J.-P. Tetienne, N. Dontschuk, D. A. Broadway, A. Stacey, D. A. Simpson, and L. C. L. Hollenberg, "Quantum imaging of current flow in graphene," *Sci. Adv.*, vol. 3, no. 4, p. e1602429, 2017.

[4] Y. Dovzhenko, F. Casola, S. Schlotter, et al., "Magnetostatic twists in room-temperature skyrmions explored by nitrogen-vacancy center spin texture reconstruction," *Nat. Commun.*, vol. 9, no. 1, p. 2712, 2018.

[5] L. Thiel, Z. Wang, M. A. Tschudin, et al., "Probing magnetism in 2D materials at the nanoscale with single-spin microscopy," *Science*, vol. 364, no. 6444, pp. 973–976, 2019.

[6] M. W. Doherty, N. B. Manson, D. Paul, F. Jelezko, J. Wrachtrup, and L. C. L. Hollenberg, "The nitrogen-vacancy colour centre in diamond," *Phys. Rep.*, vol. 528, no. 1, pp. 1–45, 2013.

[7] L. Rondin, J.-P. Tetienne, T. Hingant, J.-F. Roch, P. Maletinsky, and V. Jacques, "Magnetometry with nitrogen-vacancy defects in diamond," *Rep. Prog. Phys.*, vol. 77, no. 5, p. 056503, 2014.

[8] P. Maletinsky, S. Hong, M. S. Grinolds, et al., "A robust scanning diamond sensor for nanoscale imaging with single nitrogen-vacancy centres," *Nat. Nanotechnol.*, vol. 7, no. 5, p. 320, 2012.

[9] M. S. Grinolds, S. Hong, P. Maletinsky, et al., "Nanoscale magnetic imaging of a single electron spin under ambient conditions," *Nat. Phys.*, vol. 9, no. 4, p. 215, 2013.

[10] J. M. Taylor, P. Cappellaro, L. Childress, et al., "High-sensitivity diamond magnetometer with nanoscale resolution," *Nat. Phys.*, vol. 4, no. 10, p. 810, 2008.

[11] C. L. Degen, "Scanning magnetic field microscope with a diamond single-spin sensor," *Appl. Phys. Lett.*, vol. 92, no. 24, p. 243111, 2008.

[12] G. Balasubramanian, I. Y. Chan, R. Kolesov, et al., "Nanoscale imaging magnetometry with diamond spins under ambient conditions," *Nature*, vol. 455, no. 7213, p. 648, 2008.

[13] J. R. Maze, P. L. Stanwix, J. S. Hodges, et al., "Nanoscale magnetic sensing with an individual electronic spin in diamond," *Nature*, vol. 455, no. 7213, p. 644, 2008.

[14] T. Wolf, P. Neumann, K. Nakamura, et al., "Subpicotesla diamond magnetometry," *Phys. Rev. X*, vol. 5, no. 4, p. 041001, 2015.

[15] J. Jeske, J. H. Cole, and A. D. Greentree, "Laser threshold magnetometry," *New J. Phys.*, vol. 18, no. 1, p. 013015, 2016.

[16] V. G. Savitski, "Optical gain in nv-colour centres for highly-sensitive magnetometry: a theoretical study," *J. Phys. Appl. Phys.*, vol. 50, no. 47, p. 475602, 2017.

[17] S. C. Rand and L. G. DeShazer, "Visible color-center laser in diamond," *Opt. Lett.*, vol. 10, no. 10, pp. 481–483, 1985.

[18] N. Manson, Private Communication.

[19] V. G. Vins and E. V. Pestryakov, "Color centers in diamond crystals: their potential use in tunable and femtosecond lasers," *Diam. Relat. Mater.*, vol. 15, nos 4–8, pp. 569–571, 2006.

[20] J. Jeske, D. W. M. Lau, X. Vidal, et al., "Stimulated emission from nitrogen-vacancy centres in diamond," *Nat. Commun.*, vol. 8, p. 14000, 2017.
[21] X.-D. Chen, L. Shen, A. Shen, et al., "Near-infrared-enhanced charge-state conversion for low-power optical nanoscopy with nitrogen-vacancy centers in diamond," *Phys. Rev. Appl.*, vol. 7, no. 1, p. 014008, January 2017.
[22] L. Hacquebard and L. Childress, "Charge-state dynamics during excitation and depletion of the nitrogen-vacancy center in diamond," *Phys. Rev.*, vol. 97, no. 6, p. 063408, 2018.
[23] R. P. Roberts, L. J. Mathieu, and G. Molina-Terriza, "Spin-dependent charge state interconversion of nitrogen vacancy centers in nanodiamonds," *Phys. Rev. B*, vol. 99, no. 17, p. 174307, 2019.
[24] E. Rittweger, K. Y. Han, S. E. Irvine, C. Eggeling, and S. W. Hell, "Sted microscopy reveals crystal colour centres with nanometric resolution," *Nat. Photonics*, vol. 3, no. 3, p. 144, 2009.
[25] D. Wildanger, J. R. Maze, and S. W. Hell, "Diffraction unlimited all-optical recording of electron spin resonances," *Phys. Rev. Lett.*, vol. 107, no. 1, p. 017601, 2011.
[26] D. Wildanger, B. R. Patton, H. Schill, et al., "Solid immersion facilitates fluorescence microscopy with nanometer resolution and sub-ångström emitter localization," *Adv. Mater.*, vol. 24, no. 44, pp. OP309–OP313, 2012.
[27] S. Arroyo-Camejo, M.-P. Adam, M. Besbes, et al., "Stimulated emission depletion microscopy resolves individual nitrogen vacancy centers in diamond nanocrystals," *ACS Nano*, vol. 7, no. 12, pp. 10912–10919, 2013.
[28] N. D. Lai, O. Faklaris, D. Zheng, et al., "Quenching nitrogen-vacancy center photoluminescence with an infrared pulsed laser," *New J. Phys.*, vol. 15, no. 3, p. 033030, 2013.
[29] E. Fraczek, V. G. Savitski, M. Dale, et al., "Laser spectroscopy of NV^- and NV^0 colour centres in synthetic diamond," *Opt. Mater. Express*, vol. 7, no. 7, pp. 2571–2585, 2017.
[30] D. S. Subedi, V. V. Fedorov, J. Peppers, et al., "Laser spectroscopic characterization of negatively charged nitrogen-vacancy (NV^-) centers in diamond," *Opt. Mater. Express*, vol. 9, no. 5, pp. 2076–2087, 2019.
[31] D. Hunger, T. Steinmetz, Y. Colombe, C. Deutsch, T. W. Hänsch, and J. Reichel, "A fiber Fabry–Perot cavity with high finesse," *New J. Phys.*, vol. 12, no. 6, p. 065038, 2010.
[32] M. Capelli, A. H. Heffernan, T. Ohshima, et al., "Increased nitrogen-vacancy centre creation yield in diamond through electron beam irradiation at high temperature," *Carbon*, vol. 143, pp. 714–719, 2019.
[33] E. Janitz, M. Ruf, M. Dimock, A. Bourassa, S. Jack, and L. Childress, "Fabry–Perot microcavity for diamond-based photonics," *Phys. Rev.*, vol. 92, no. 4, p. 043844, 2015.
[34] C. Bradac, T. J. Mattias, M. Van Breugel, et al., "Room-temperature spontaneous super radiance from single diamond nanocrystals," *Nat. Commun.*, vol. 8, no. 1, p. 1205, 2017.
[35] N. B. Manson, M. Hedges, M. S. J. Barson, et al., "NV^-–N^+ pair centre in 1b diamond," *New J. Phys.*, vol. 20, no. 11, p. 113037, 2018.
[36] F. M. Hrubesch, G. Braunbeck, S. Martin, F. Reinhard, and M. S. Brandt, "Efficient electrical spin readout of NV^- centers in diamond," *Phys. Rev. Lett.*, vol. 118, no. 3, p. 037601, 2017.
[37] J. P. Tetienne, L. Rondin, P. Spinicelli, et al., "Magnetic-field-dependent photodynamics of single NV defects in diamond: An application to qualitative all-optical magnetic imaging," *New J. Phys.*, vol. 14, no. 10, p. 103033, 2012.
[38] T.-L. Wee, Y.-K. Tzeng, C.-C. Han, et al., "Two-photon excited fluorescence of nitrogen-vacancy centers in proton-irradiated type ib diamond," *J. Phys. Chem.*, vol. 111, no. 38, pp. 9379–9386, 2007.
[39] Y. Dumeige, J.-F. Roch, F. Bretenaker, et al., "Infrared laser threshold magnetometry with a NV doped diamond intracavity etalon," *Opt. Express*, vol. 27, no. 2, pp. 1706–1717, 2019.
[40] I. Meirzada, Y. Hovav, S. A. Wolf, and N. Bar-Gill, "Negative charge enhancement of near-surface nitrogen vacancy centers by multicolor excitation," *Phys. Rev. B*, vol. 98, no. 24, p. 245411, 2018.
[41] A. T. Collins, "The fermi level in diamond," *J. Phys. Condens. Matter*, vol. 14, no. 14, p. 3743, 2002.
[42] P. Siyushev, H. Pinto, M. Vörös, A. Gali, F. Jelezko, and J. Wrachtrup, "Optically controlled switching of the charge state of a single nitrogen-vacancy center in diamond at cryogenic temperatures," *Phys. Rev. Lett.*, vol. 110, no. 16, p. 167402, Apr. 2013.
[43] W. J. P. Van Enckevort and E. H. Versteegen, "Temperature dependence of optical absorption by the single-substitutional nitrogen donor in diamond," *J. Phys. Condens. Matter*, vol. 4, no. 9, p. 2361, 1992.
[44] G. Davies, S. C. Lawson, A. T. Collins, A. Mainwood, and S. J. Sharp, "Vacancy-related centers in diamond," *Phys. Rev. B*, vol. 46, no. 20, pp. 13157–13170, Nov. 1992.
[45] T. Frank, *Springer Handbook of Lasers and Optics*, Springer Science & Business Media, 2012. https://doi.org/10.1007/978-3-642-19409-2.
[46] B. Aull and H. Jenssen, "Vibronic interactions in ND:YAG resulting in nonreciprocity of absorption and stimulated emission cross sections," *IEEE J. Quant. Electron.*, vol. 18, no. 5, pp. 925–930, 1982.